Frontogenesis in the Presence of Surface Heating

G. W. KENT MOORE

Department of Physics, University of Toronto, Toronto, Ontario Canada

(Manuscript received 2 May 1989, in final form 30 June 1990)

ABSTRACT

Observations indicate that frontal zones that form in the presence of strong surface sensible heating have a structure that is markedly different from those that form adiabatically. These differences include: a highly asymmetric low-level jet, the presence of an isothermal pool of warm air in the vicinity of the jet, an enhancement of the baroclinicity on the cold side of the jet, and an extension of the region of low Richardson number into the cold air.

In order to investigate the dynamics responsible for these differences, a Lagrangian model was developed that allowed for the incorporation of a surface sensible heat flux parameterization into the semigeostrophic theory of deformation induced frontogenesis. The model was tested by comparison against the analytic solution that exists in the special case of adiabatic frontogenesis in a constant potential vorticity fluid. Having established the validity of the model, the effects that surface sensible heating has on frontogenesis in a nonuniform potential vorticity fluid were investigated. It is shown that the frontal zones generated by means of the model have the same structural characteristics as those of the observed fronts which formed in the presence of strong surface sensible heating.

It is also shown that surface heating can lead to both an increase in the maximum baroclinicity and a reduction in the minimum stratification associated with a frontal zone. Both of these modifications can be expected to result in an increase in the rate at which instabilities along the front can develop. This then provides for an *indirect mechanism* by which surface heating contributes to the development of cyclonic disturbances by modifying the background flow rather than by direct interaction with the growing cyclone.

1. Introduction

In this paper, the effect that surface sensible heat fluxes have on the formation and maintenance of synoptic-scale frontal zones will be investigated. An excellent example of this effect has recently been provided by Reed and Duncan (1987). They describe a quasi-two-dimensional frontal zone that formed over the Norwegian Sea during March 1985. This particular frontal zone was the result of the action of a large-scale deformation field and is interesting because of the fact that a family of polar lows was observed to develop along it. Moore and Peltier (1989b) have shown that this development is the result of the cyclone-scale mode of baroclinic instability identified in the analysis of Moore and Peltier (1987). Figure 1a shows the cross section perpendicular to the front of the normal (along-front) velocity V and potential temperature θ fields for this zone. The front was oriented such that the cross section shown went from the coast of Greenland to that of Norway. The cross section was derived from the operational analysis done by the European Center for Medium Range Weather Forecasts. This analysis was not able to resolve the individual polar lows and as a result it provides a representation of the synoptic-scale environment in which the storms developed. The Richardson number field:

$$\mathrm{Ri} = (g/\theta_0)[\partial_z\theta/(\partial_z V)^2] \tag{1}$$

and the static stability field:

$$S = \partial_z\theta \tag{2}$$

associated with this baroclinic zone are displayed in Fig. 1b. The arrow in both panels of this figure indicates the storm track of the lows.

In the winter months, there is a narrow tongue approximately 800 km wide of relatively warm water present in the Norwegian Sea (Forbes and Lottes 1985; Rasmussen 1985). The average sea surface temperature in the tongue is near 5°C. To the east and west, the warm water is bounded by land masses or ice sheets where the surface temperature is colder than 0°C. The surface temperatures to the west, i.e., those associated with Greenland, are considerably colder than those associated with Norway to the east (Reed and Duncan 1987). The region is thus characterized by large gradients, most notably between Greenland and the Norwegian Sea, in the surface temperature. The surface air temperatures over the Norwegian Sea during the time that this front formed were considerably colder

Corresponding author address: Dr. G. W. K. Moore, Department of Physics, University of Toronto, Toronto, Ontario, Canada M5S 1A7.

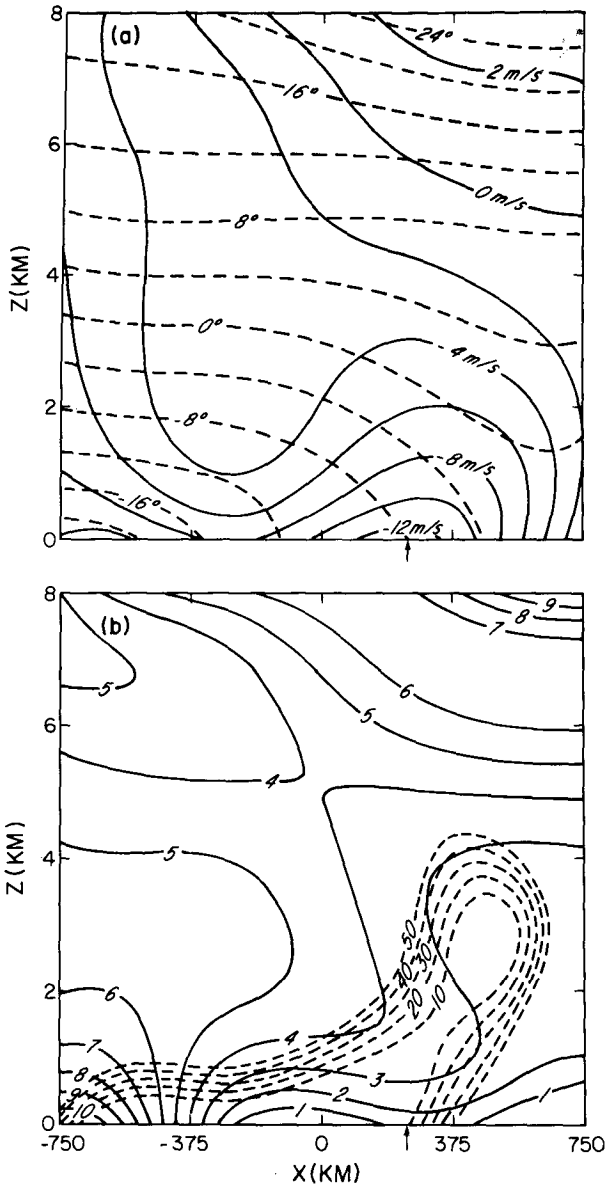

FIG. 1. (a) Cross sections of potential temperature (dashed lines, °C) and along-front velocity (solid lines, m s^{-1}) representing the frontal zone described by Reed and Duncan (1987). (b) Cross sections of static stability (solid lines, °C km^{-1}) and Richardson number (dashed lines) derived from the fields in Fig. 1a.

than 0°C. As a result, there was a significant air–surface temperature contrast that resulted in a strong surface sensible heat flux.

The structure of this frontal zone is very different from that of a typical adiabatic Hoskins–Bretherton front, such as the one illustrated in Fig. 2. The most obvious difference is the relative shallowness of the front in Fig. 1 as compared to that in Fig. 2. This is not, however, an important difference as it simply reflects the fact that the initial states out of which the fronts evolved were different. Neglecting the difference in depth, or alternatively focusing attention on the lower troposphere, it is seen that there are still features present in Fig. 1 that are absent in Fig. 2. These include: the isothermal pool of warm air to the right (south) low-level jet, the reduced static stability in the vicinity of the jet, the strong meridional asymmetry in the jet itself, and the extension of the region of low Ri into the cold air.

It will be demonstrated that by incorporating a parameterization of the surface sensible heat flux into the

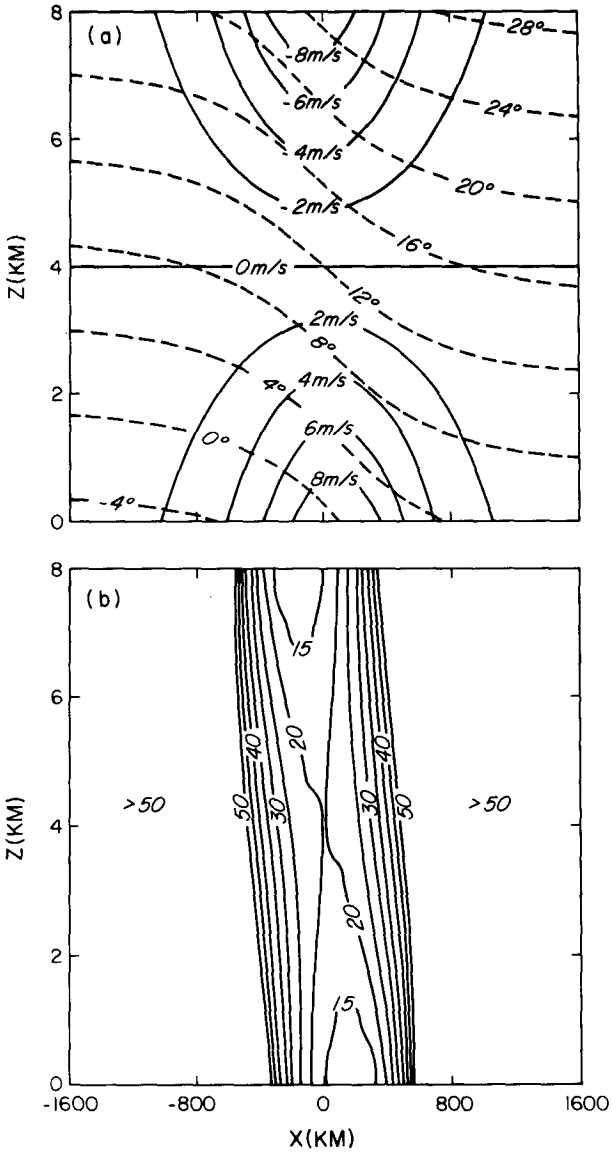

FIG. 2. Cross sections of potential temperature (dashed lines, °C) and along-front velocity (solid lines, m s^{-1}) associated with the deformation induced frontal zone C222 that forms in a constant potential vorticity fluid. (b) Cross section of the Richardson number field derived from the fields in Fig. 2a. Note the change in horizontal scale between Fig. 1 and 2. See text for a description of the parameters that describe the initial state.

semigeostrophic theory of Hoskins and Bretherton (1972), it is possible to generate deformation-induced frontal zones that have all of the features of the baroclinic zone displayed in Fig. 1. As will be shown, a key ingredient in this successful parameterization is a surface temperature distribution which incorporates the strong contrast between the cold Greenland land mass and the warm waters of the Norwegian Sea.

One of the advantages, though it is seldom used, of the semigeostrophic theory of frontogenesis is that the resulting equations can be written as Lagrangian conservation laws. The incorporation of diabatic processes generates source/sink terms that greatly complicate their solution. Rather than attempting to deal with these additional terms in the Lagrangian sense, most investigations of frontogenesis modified by diabatic processes have chosen to solve the resulting equations in the Eulerian sense (Williams et al. 1981; Mak and Bannon 1984; Thorpe and Emmanuel 1985; Chan 1988). In this paper, a different approach has been taken and a Lagrangian model has been developed. As shall be demonstrated, the construction of such a model is relatively simple. Unlike the Lagrangian model described in Cullen (1983) and Cullen and Purser (1984), which is restricted to zero potential vorticity fluids, the model developed in this paper makes no assumptions as to the potential vorticity distribution in the fluid. The model is described in the following text.

2. Description of the model

In this paper, the effect that surface sensible heating has on the process of frontogenesis will be investigated. The fronts studied are those that form as a result of the action of a hyperbolic deformation field on an initial state with a very weak cross-front temperature gradient. Following Hoskins and Bretherton (1972), the geostrophic momentum approximation will be made. A coordinate system will be employed in which the x-axis is in the cross-front direction, the y-axis is in the along-front direction, and the "pseudoheight" is used as a vertical coordinate. The solution of this problem is greatly facilitated by the transformation into geostrophic coordinates defined by:

$$X = x + V/f, \quad Z = z \quad \text{and} \quad T = t.$$

In the transformed space, the structure of the frontal zone is described in terms of the potential temperature θ, potential vorticity q:

$$q = \zeta(\partial\theta/\partial Z), \tag{3}$$

and cross-front streamfunction Ψ fields. The evolution of these fields is determined by the following system:

$$D\theta/DT = E, \tag{4}$$

$$Dq/DT = \xi(\partial E/\partial Z) \tag{5}$$

and

$$f^2\frac{\partial^2\Psi}{\partial Z^2} + \frac{g}{f\theta_0}\frac{\partial}{\partial X}\left[q\frac{\partial\Psi}{\partial X}\right] = -\frac{2\alpha(t)g}{\theta_0}\frac{\partial E}{\partial X}. \tag{6}$$

In the above, α represents the magnitude of the applied deformation field and E represents the diabatic heating function.

For the case in which the diabatic heating vanishes, θ and q are conserved following parcel trajectories. It can be shown that in this case time enters into the problem only through the total deformation applied, which can be conveniently expressed in terms of the deformation length scale L_d. An analytic solution is possible for this case when the frontogenesis occurs in a constant potential vorticity fluid. For more general distributions of q, an analytic solution is not possible and the numerical methods developed by Buzzi et al. (1981) or Moore (1987) must be employed.

As the primary focus of this paper is in those cases in which the process of frontogenesis is modified by the presence of surface sensible heating, neither θ nor q will be conserved and the methods mentioned previously are inappropriate. To solve the frontogenesis problem in this instance, the Lagrangian perspective has been adopted. One advantage of this approach is that as the deformation acts to reduce the width of the front, it also leads to a contraction in the lateral boundaries of the computational domain. This leads to an *effective* increase in the lateral resolution as time goes on. The procedure followed is quite simple. A regular rectangular lattice of fluid elements (X_{ij}, Z_{ij}) is defined on the domain from $(-L, 0) < (X, Z) < (L, H)$. Given the initial distributions of potential temperature and vorticity, the values of these fields θ_{ij} and q_{ij} associated with each fluid element are defined. The displacements of the fluid elements $(\Delta X_{ij}, \Delta Z_{ij})$ that occur during the time step from $T = 0$ to $T = \Delta T$ can be found by solving (6) for the cross-front streamfunction Ψ. At the new positions of the fluid elements, $(X_{ij} + \Delta X_{ij}, Z_{ij} + \Delta Z_{ij})$, the new values of θ_{ij} and q_{ij} can then be calculated from (4) and (5).

This process can in principle be applied repeatedly to advance the solution in time. The only difficulty with it arises from the fact that the fluid elements will not remain on a rectangular lattice. The nonregularity of the lattice makes the solution of the elliptic equation for the streamfunction (6) extremely difficult. This particular problem can be overcome by taking the distributions of θ and q as defined on the nonrectangular lattice and mapping them onto a rectangular lattice. As such, it represents a variation on the mesh restructuring method discussed by Fritts and Boris (1979). After this operation has been completed, (6) may then be readily solved and the procedure previously described, with θ and q defined on the new rectangular lattice, can be repeated to advance the solution in time.

The mappings between the nonrectangular and the

rectangular grids is a process that has the *potential* of introducing numerical diffusion into the system. As in dealing with an inviscid system in which large gradients develop, the existence of a diffusive process that is numerical in origin is most troublesome. To ensure that this diffusion does not contaminate the solution, the mappings were accomplished by means of an algorithm developed by Akima (1978). The algorithm computes a continuously differentiable interpolant that is locally described in terms of bivariate quintic polynomials to scattered data in the X–Z plane. In the present context, the scattered data represent either the θ or q fields defined on the irregular lattice. In addition, the interpolant is required to pass through all the data points and to preserve the local curvature implied by the data. As will be seen, these properties have the cumulative effect of minimizing the diffusive tendency inherent in the mesh restructuring.

The solution to the elliptic equation for Ψ, (6), at each time step was found by means of an implementation of the multigrid method (Brandt 1985). This method uses a iterative scheme, in this case Gauss-Seidel line relaxation, and a hierarchy of grids of varying resolution to solve for Ψ. The primary advantage of the multigrid method is its greater efficiency when compared to classical relaxation methods.

To initialize the model, distributions of potential vorticity and temperature are required. These two fields are related through (3) which may be integrated to yield:

$$\theta(X, Z, 0) = \theta_s(X) + \frac{1}{f}\int_0^Z q(X, Z', 0)dZ'. \quad (7)$$

The initial air temperature at the surface θ_s is taken to be adequately described by an inverse tangent profile of the form:

$$\theta_s(X) = (R/\pi)\tan^{-1}(X/L_s), \quad (8)$$

in which L_s is a measure of the initial scale of the surface temperature gradient and R is the total temperature contrast across the front. In order for the fronts that form to be well isolated from the lateral boundaries of the domain, it is required that $L_s < L$. The actual initial states used in this paper are described in section 3.

The incorporation of the surface heat flux into a balanced model, such as the one described here, is complicated by the fact that the model is incapable of describing the boundary layer physics responsible for the transfer. Hoskins and Bretherton (1972) and others (including: Young 1973; Blumen 1980; Wu and Blumen 1982) have developed procedures by which frictional processes, as described by Ekman theory, have been successfully coupled into semigeostrophic theory. The same can not be said for thermal processes. Indeed it is only with the recent work of Cullen (1989) that any attempt has been made to parameterize such processes. It is however unclear whether Cullen's parameterization, which was developed for sea-breeze fronts, is valid for deformation induced frontal zones under investigation herein. Given this uncertainty along with the fact that oceanic boundary layers in which frictional processes are likely to be rather weak are being considered, no attempt has been made to include an explicit boundary layer in the model. Rather, a bulk aerodynamic formula will be used to determine the magnitude of the heating and then distribute it throughout the interior of the fluid in a prescribed manner. As shall be seen, this admittedly simple parameterization nevertheless produces surprisingly realistic results.

Following the standard bulk aerodynamic formula (Gill 1982), it has been assumed that the sensible heat flux Q has the following form:

$$Q = \rho C_p C_H V_s \Delta\theta, \quad (9)$$

in which: ρ is the density of air; C_p is the specific heat at constant pressure; C_H is the nondimensional exchange coefficient which is assumed to have the value of 0.001; V_s is the magnitude of surface wind; and $\Delta\theta$ is the air–surface temperature contrast defined as follows:

$$\Delta\theta = ST(x) - \theta(x, 0, T). \quad (10)$$

Various distributions of surface temperature $ST(x)$ were employed in this study. In addition to cases in which it was a constant, cases were considered in which there was a pronounced gradient in this field. The investigation of the latter cases was motivated by the conditions typical of the Norwegian Sea in the winter. The surface temperature distributions employed in this paper are all described in terms of the following function:

$$ST(x) = (ST_{mx} + ST_{mm})/2 + (ST_{mx} - ST_{mn})\tan^{-1}(x/L_{st}), \quad (11)$$

in which L_{st} represents the characteristic length scale for change in the surface temperature distribution, while ST_{mx} and ST_{mn} represent the maximum and minimum surface temperatures, respectively. In Fig. 3, the various distributions used in this study are displayed. The distributions have been labeled by the ordered pair (ST_{mn}, ST_{mx}). All distributions have L_{st} = 200 km. From this figure, it is noted that all the variable distributions are characterized by cold temperatures for large negative values of x. This corresponds to the fact that there is an ice sheet to the west of the tongue of warm water in the Norwegian Sea.

It should be noted that this parameterization of the surface temperature distribution assumes that the ocean is an infinite heat source. In reality the oceanic mixed layer is not passive and as heat is removed its temperature will change. The process whereby the ocean responds to its role as an atmospheric heat source will be investigated in subsequent work.

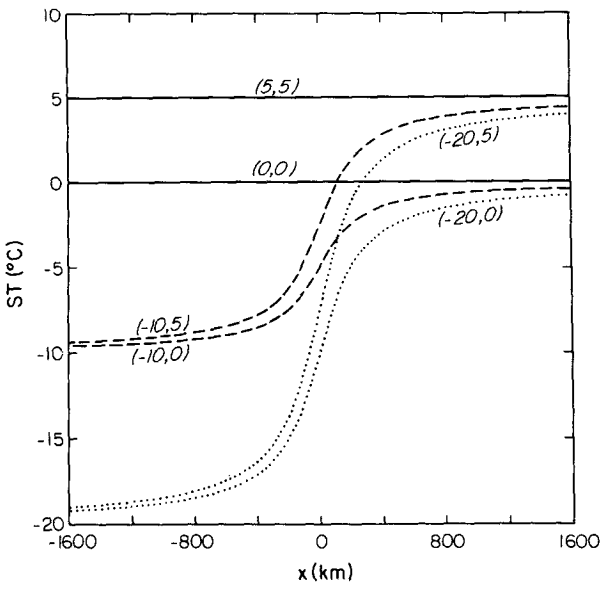

FIG. 3. Distributions of surface temperature ST as a function of x. Curves are labeled by the ordered pair (ST_{mn}, ST_{mx}).

There are several difficulties implicit in the dependence of the surface heat flux on wind speed as defined by (9). As it stands, V_s includes a contribution from the deformation field and as such, Q varies in the along-front (y) direction. This has the unwanted effect of rendering the assumption as to the two-dimensionality of the frontal fields invalid. A further complication results from the fact that for large values of x or y, V_s itself becomes large as a result of the contribution from the deformation field. The use of a hyperbolic deformation field with its concomitant unbounded velocities is an obvious simplification to the actual deformation fields found in the atmosphere. The usefulness of this approximation, with regards to the theory of two-dimensional frontogenesis arises, out of the fact that the *unphysical behavior of the deformation field does not, in general, impact on the frontal circulations that are generated by this theory.* This is clearly not the case when surface heating is included.

One could conceivably circumvent this problem by employing a more realistic representation of the mechanism by which frontogenesis occurs. This approach is certainly possible as is illustrated by the three-dimensional frontogenesis models developed by Hoskins and West (1979), Peltier et al. (1990), and others. The use of a more complex three-dimensional model would however detract and make more obscure the goal of this present study, which is to identify the ways in which surface heating acts to modify the process of frontogenesis. The only other alternative is to modify V_s so as to remove the contribution from the applied deformation field. Although this approach represents an obvious simplification, it will serve to elucidate the mechanisms by which surface heating modifies the process of frontogenesis. In subsequent work, this point will be reconsidered and the effects of surface heating within the context of a more realistic representation of the frontogenesis process will be investigated.

To conclude the discussion of the surface heat flux parameterization, a description of how the heat from the surface is distributed throughout the interior of the fluid must be given. As the model is unable to resolve the convection responsible for this, it has been assumed that it is distributed in a manner similar to that used in CISK parameterizations (Mak and Bannon 1984). That is, the heat is distributed in the vertical according to a prescribed profile $h(z)$. Accordingly, the diabatic heating function E has the following form:

$$E(x, z, t) = C_H V_s(x, t)\Delta\theta(x, t)h(z). \quad (12)$$

The heating profile is defined in terms of a depth of heating L_z as follows:

$$h(z) = \begin{cases} (2/L_z) - (6z^2/L_z^3) + (4z^3/L_z^3); & z \leq I_z \\ 0; & z > L_z \end{cases}. \quad (13)$$

This profile, which has its maximum at $z = 0$, has been constructed so that it and its first derivative are continuous functions of z. Furthermore, it has been normalized such that its integral between 0 and L_z is unity. For all cases considered, the depth of heating L_z was taken to be 4 km. Varying L_z will lead to qualitative but not quantitative changes in the results to be presented.

3. Results

This section will describe the integrations that have performed with the Lagrangian model described in the previous section. In order to establish the validity of this model, the adiabatic fronts that form in a constant potential vorticity fluid will be considered first. The results obtained will be compared to those found with the analytic solution described by Hoskins and Bretherton (1972). Having demonstrated this, the effects that surface sensible heating has on the fronts which form in a nonuniform potential vorticity fluid will be considered. The results obtained from these simulations will be compared to observations of frontal zones which have been modified by surface sensible heating.

For the case of frontogenesis in an adiabatic constant potential fluid, the same initial state as was employed by Hoskins (1971) and Moore and Peltier (1987) has been chosen. The initial domain has a width $L = 8000$ km and a depth $H = 8$ km. The potential vorticity q has the value of 3×10^{-7} °C m^{-1} s^{-1} throughout the domain. The initial surface temperature distribution is characterized by $L_s = 1600$ km and $R = 12$°C. In Table 1, several indicators of frontal intensity obtained with the Lagrangian model are compared to those from the analytic solution of Hoskins and Bretherton (1972).

TABLE 1. A comparison of the analytic and Lagrangian model solutions for the case of deformation induced frontogenesis in a constant potential vorticity fluid.

Name	Grid size ($NX \times NZ$)	Time step (ΔT, s)	Deformation rate	Max V (m s^{-1})	Min Ri	Max W (m s^{-1})
Analytic			constant	9.9	10.1	0.27
C112	64 × 32	1000	constant	10.1	10.7	0.27
C222	32 × 16	1000	constant	10.1	11.5	0.27
C221	32 × 16	500	constant	10.1	11.6	0.26
V222	32 × 16	1000	variable	10.1	11.6	0

The results displayed were obtained after an integration of 1.6 days with a constant deformation rate of $\alpha = 10^{-5}$ s^{-1}. Results from the Lagrangian model are shown for various grid sizes and time steps. Also shown are results obtained after a period of 3.2 days with a variable deformation rate given by

$$\alpha(t) = \begin{cases} 10^{-5}(1 - T/3.2 \text{ days}) \text{ s}^{-1}, & T \leq 3.2 \text{ days} \\ 0, & T > 3.2 \text{ days.} \end{cases} \quad (14)$$

It can be demonstrated that both the constant and variable deformation rate cases have the same deformation length scale L_d of 400 km. It follows that the only difference between the two solutions should be in the intensity of the cross-front circulation.

From the table, it can be seen that the results obtained with the Lagrangian model agree favorably with those from the analytic solution. Furthermore, the Lagrangian model results shows very little sensitivity to either grid size or time step. Also, as required by the theory, one can see that the integrations are independent of the functional form of the deformation rate. In Fig. 2, the hydrodynamic fields associated with the front that formed during the model run C222 at $L_d = 400$ km are displayed.

As described in section 2, the mesh restructuring technique that has been employed has the potential of introducing numerical diffusion into the model. The comparison described above provides strong evidence that the diffusive properties of the mesh restructuring have indeed been minimized. As a further test, one can compare the deformation length scale at which the front collapses in this model (60.4 km) against that of the analytic solution (61.5 km). It should be emphasized that the solution in the transformed space remains well behaved at all times and that the *singularity results from its transformation back into physical space.* Notwithstanding this point, the transformation makes use of the solution's along-front velocity field and hence an accurate prediction of the time of collapse requires an accurate solution in the transformed space. The close agreement between the values of L_d at which the fronts collapse is yet another indication as to the ability of our Lagrangian model to faithfully describe the process of deformation induced frontogenesis.

The effect that surface heating has on the process of frontogenesis will now be investigated. Because these effects will be limited to the lower troposphere, an initial state has been chosen with a nonuniform potential vorticity distribution that has no horizontal temperature gradient along the tropopause ($Z = H$). The form of the initial potential vorticity distribution used is the same as that employed by Moore (1987):

$$q(X, Z, 0) = [(q_s + q_t)/2] + [(q_s - q_t)/2] \tanh\{[Z - Z_t(X)]/\delta\}, \quad (15)$$

where q_t and q_s represent typical tropospheric and stratospheric potential vorticities, δ is a measure of the depth of the transition zone over which there is a large gradient in q, and Z_t is the height of this transition zone. The condition that the potential temperature along the upper lid is the constant θ_H fixes the height of the transition zone. The parameters in (15) were chosen so as to result in an initial state that is representative of conditions found in the Norwegian Sea (Reed and Duncan 1987). The particular values used are as follows:

$$q_t = 1 \times 10^{-7} \text{ °C m}^{-1} \text{ s}^{-1},$$

$$q_s = 2 \times 10^{-7} \text{ °C m}^{-1} \text{ s}^{-1},$$

$$\theta_H = 32\text{°C} \quad \text{and} \quad \delta = 2 \text{ km}.$$

For this case, the surface temperature distribution was characterized by $L_s = 1600$ km and $R = 18$°C. The vertical profiles of the initial potential vorticity and potential temperature distributions at $X = -L$, 0 and L are displayed in Fig. 4. From this figure one can see that, in accordance with observations (Mansfield 1974; Reed and Duncan 1987), there is an increase in stratification as one goes from the warm side ($X = L$) to the cold side ($X = -L$) of the front. For the integrations with this initial state, a time step of 1000 s (16.67 min.) and a 32 × 16 grid were used.

Figure 5 shows the along-front velocity V and potential temperature θ fields associated with fronts that form for various surface heating scenarios. The deformation length scale for all of these fronts has the value of 400 km. As previously described, the surface temperature distributions are identified by the ordered pair (ST_{mn}, ST_{mx}). Inspection of the results presented in

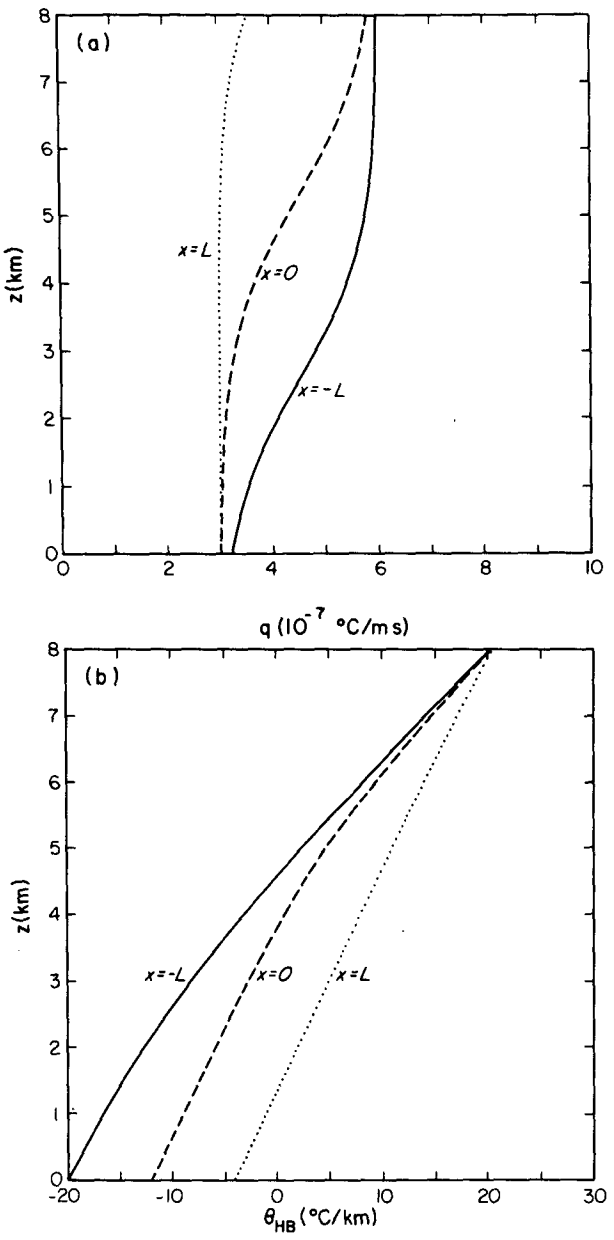

FIG. 4. Vertical profiles of the potential vorticity q (a) and potential temperature θ (b) fields associated with the nonuniform potential vorticity initial state.

this figure shows that there are important differences between the front that forms when there is no surface heating and those that form in the presence of such heating. The most striking of these differences is in the symmetry or lack thereof of the low-level jet. In the no heating case, the along-front velocity field exhibits a high degree of symmetry about the front's axis of maximum baroclinicity ($x \sim 0$). This symmetry is not however an exact one and it is broken by the nonlinearities retained by the geostrophic momentum approximation. The other panels in this figure show that the inclusion of surface heating results in an even more dramatic breaking of this symmetry. This is manifested by a reduction in the vertical wind shear on the warm side of the front and an enhancement of it on the cold side. Another difference that can be attributed to surface heating is the reduction in the stratification associated with the front.

The differences described so far are ones that are common to all cases in which the fronts form in the presence of surface heating. As such, they are independent of the specific surface temperature distribution employed. Comparison of Fig. 5b with Figs. 5c,d show that the surface temperature distribution can also have an impact of the structure of the fronts that form. One can see that in the constant surface temperature case, there is a reduction in the maximum vertical shear of the along-front wind as compared to the no heating case. Because the flow is assumed to be in thermal wind balance, the reduction in maximum vertical wind shear is associated with a reduction in the maximum baroclinicity associated with the front. For the cases in which the surface temperature is nonconstant, there is an enhancement as compared to the no heating case in both the maximum vertical shear and baroclinicity.

Further information on the effect that surface heating has on the structure of frontal zones can be obtained by examining the time history of two indicators of frontal intensity, minimum static stability, and the maximum baroclinicity. The time histories of these two quantities are shown in Figs. 6 and 7, respectively. Results are shown for the control case, in which there is no heating, and for various surface temperature distributions.

From Fig. 6, one sees that in all the cases the minimum stratification is a decreasing function of time. There are two processes that are responsible for this behavior. As frontogenesis proceeds, scale contraction implies that the relative vorticity associated with the front must increase. From the definition of q this requires that, in the absence of diabatic processes, the stratification must decrease as a function of time. In addition to this adiabatic effect, the conservation laws for θ and q, indicate that the presence of surface heating will result in a further reduction in the stratification. From Fig. 6, it is seen that for the cases presented, the latter effect is the more pronounced. It is possible to categorize the results for the various heating cases according to the maximum surface temperature ST_{mx}. That is, the higher the value of ST_{mx}, the greater the reduction as compared to the control case in the stratification. Within each group in which ST_{mx} is a constant, the cases are further stratified according to the minimum surface temperature ST_{mn}. This dependence on ST_{mx} and ST_{mn} suggests that the reduction in stratification is a result of the average surface temperature and is thus independent of the specific form chosen.

Figure 7 shows that in all cases the maximum baroclinicity is an increasing function of time. This can be

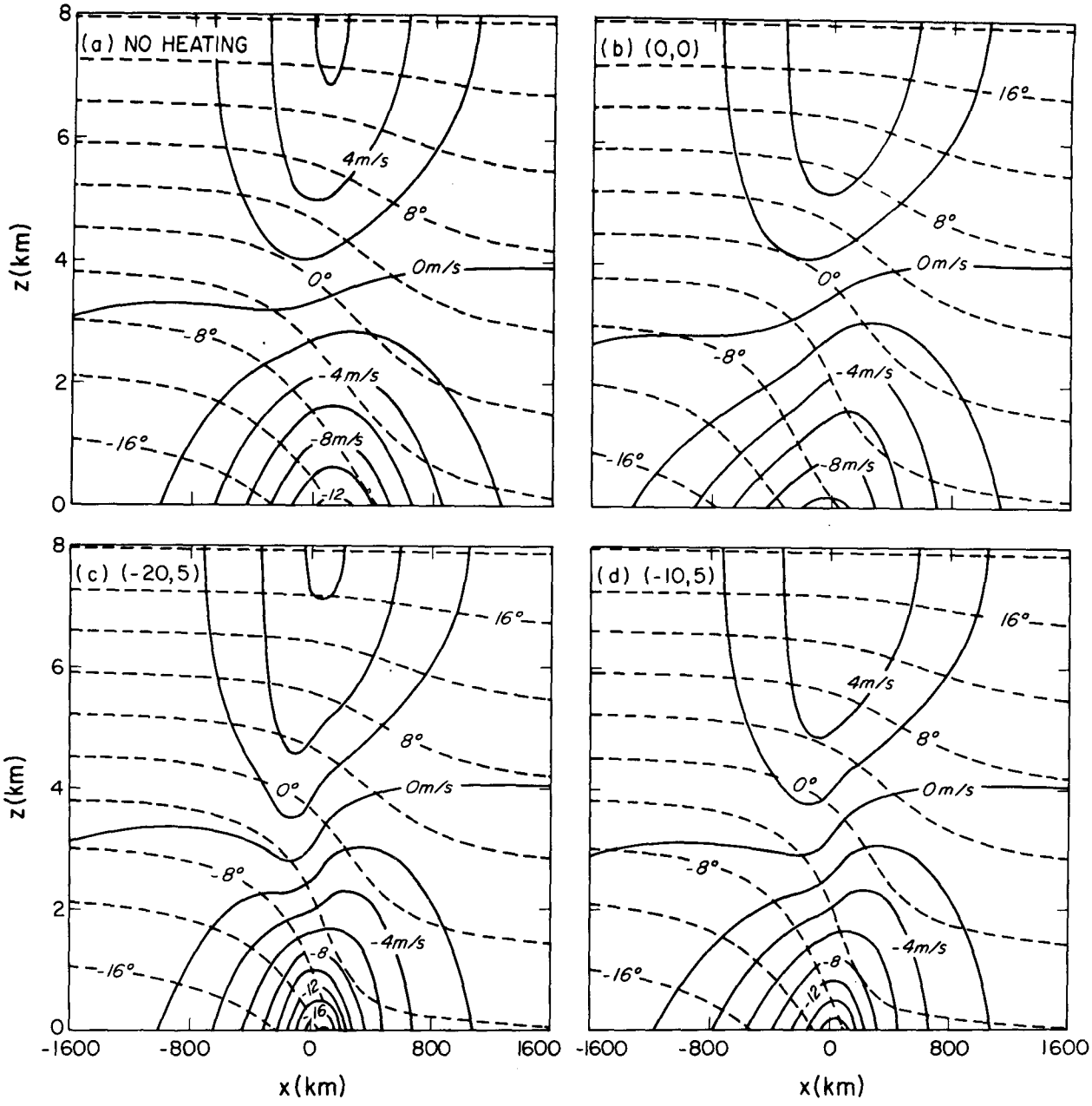

FIG. 5. Cross sections of the potential temperature (dashed lines, °C) and along-front velocity V (solid lines, m s^{-1}) associated with the deformation induced frontal zones that form in the nonuniform potential vorticity fluid after 1.6 days. The surface temperature distributions responsible for the modifications in the frontal zones in panels b–d are described in terms of the ordered pair (ST_{mn}, ST_{mx}).

partially understood as resulting from the deformation field's concentration of the cross-frontal temperature contrast. In addition, it is seen that surface heating can act either to augment or to diminish the frontogenetic effect of the deformation field. From the results presented in Fig. 7, it appears that the key criterion that distinguishes between these two possible outcomes is the uniformity or nonuniformity of the surface temperature distribution. For cases in which the surface temperature is constant, the effect of heating is to reduce the maximum baroclinicity associated with the front. In the cases in which the surface temperature is nonuniform, there is a direct correlation between the total temperature contrast ($ST_{mx} - ST_{mx}$) and maximum baroclinicity. The results presented in Fig. 7 suggest that the specific form of the surface temperature distribution has a marked effect on the maximum baroclinicity associated with a frontal zone that has been subject to surface heating.

This strong dependence on the form of the surface

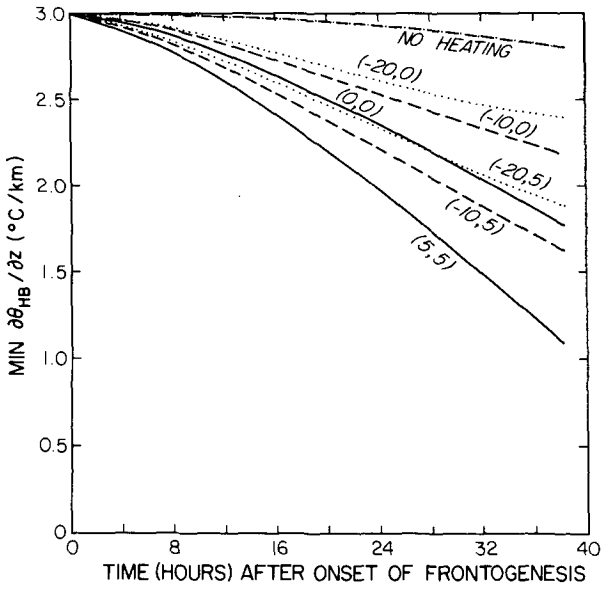

FIG. 6. The minimum stratification (°C km^{-1}) as a function of time for various fronts that have been subject to surface heating during frontogenesis. Also shown is the minimum stratification in the control case in which there was no heating.

temperature distribution can be understood as follows. The magnitude of the heating is a function of both V_s and $\Delta\theta$. The surface wind, by definition, is always a maximum in the vicinity of the jet maximum. In contrast, the region in which $\Delta\theta$ is a maximum is a function of the surface temperature distribution. In cases in which the surface temperature is a constant, $\Delta\theta$ will be largest where the surface air temperatures are coldest, that is on the cold side of the front. In the variable surface temperature cases, the cold surface temperatures on the cold side of the front have the effect of eliminating temperature contrasts in this region. As a result, $\Delta\theta$ will be largest in the vicinity of the jet maximum. It follows that the position of the region of maximum heating is a strong function of the surface temperature distribution. In the variable surface temperature cases, its location in the vicinity of the jet maximum has the effect of decreasing the temperature gradients on the warm side of the front and increasing them on the cold side. This increase occurs in the region in which the gradients are already large and, thus, leads to an *increase in the maximum baroclinicity* associated with the front. In the constant surface temperature cases, the region of maximum heating is situated on the cold side of the front. Its location is *such as to reduce the maximum baroclinicity associated with the front.*

So far cases have been described in which the surface heating has been active while the deformation field was concentrating the cross-front temperature contrast. These cases correspond to the scenario of frontogenesis occuring in a region in which there is a surface sensible heat flux. It is also possible that the surface heat flux could become important only after the applied deformation had ceased. To consider this scenario, the nonuniform potential vorticity initial state previously described was subject to the time dependent deformation rate (14). While the deformation is nonzero, i.e., $T < 3.2$ days, there is no surface heating. After 3.2 days, the deformation vanishes and the surface heating is turned on. One of the advantages of studying this sort of scenario is that there is *no contribution* from the deformation field to the surface wind speed V_s. Recall that it was the y dependence and the unbounded behavior of the deformation field wind components at large x that led to problems in the parameterization of the surface heat flux. This problem no longer exists and as a result, no approximation is involved in the choice of surface wind field to employ.

Figure 8 shows that along-front velocity V and potential temperature θ fields associated with the fronts that have formed by the above scenario. The no heating case, Fig. 8a, represents the steady-state control case. It has, as required by the theory, exactly the same structure as that shown in Fig. 5a. All the other fronts in this figure, 8b–d, have been subject to a further two days of surface heating. From this figure, it is seen that surface heating has again led to a breaking in the symmetry of the along-front wind field. As was found in Fig. 5, this is associated with a reduction in the vertical wind shear on the warm side of the front and an enhancement of it on the cold side. There is also an overall reduction in the stratification of the fronts. Comparison of Figs. 5 and 8 reveal a great deal of similarity between frontal zones, which have been subject to heating, that

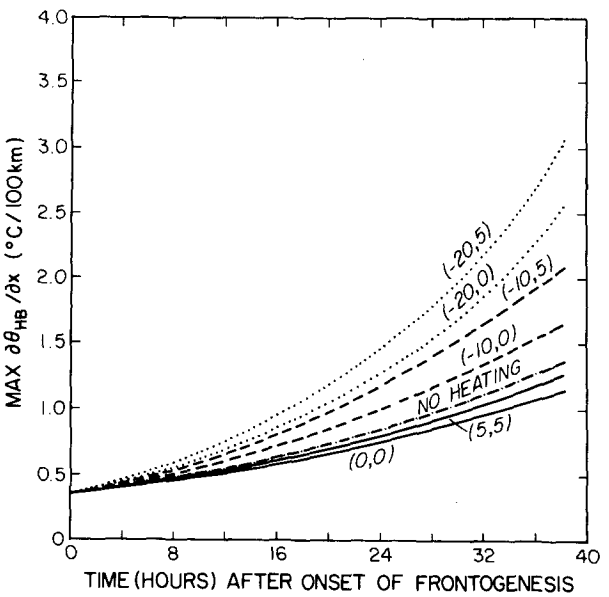

FIG. 7. As in Fig. 6, but for the maximum baroclinicity [°C (100 km)$^{-1}$].

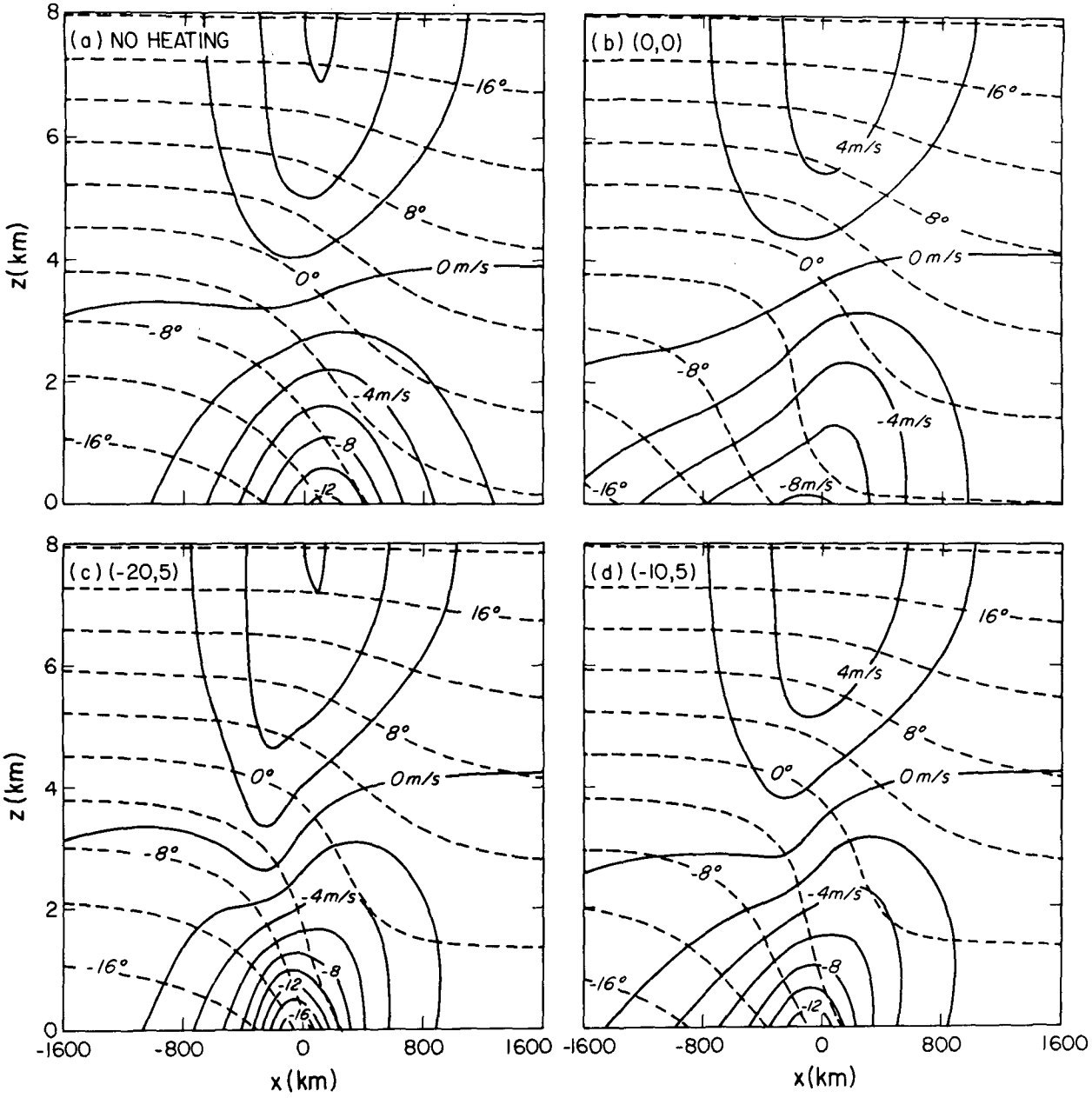

FIG. 8. As in Fig. 5, but for the fronts that have been subject to surface heating for a period of two days after the cessation of deformation induced frontogenesis.

arise out of same surface temperature distribution. The only systematic difference can be attributed to the fact that for the fronts in Fig. 8 the integrated heat flux is larger than that associated with the corresponding front in Fig. 5. This leads to more pronounced changes in the fronts of Fig. 8 as compared to those of Fig. 5.

In Fig. 9, a comparison of the potential vorticity field associated with the frontal zones of Figs. 8a and d is illustrated. As is expected from the above discussion concerning modifications to the static stability field, it is clear from this figure that in the interior of the fluid heating has produced a region of reduced q. The reason why the minimum in q is above the surface follows from the fact that the change in q following fluid motion (5) is a function of the vertical derivative of the diabatic heating.

The Richardson number field combines information about both the baroclinicity and stratification associated with a frontal zone. Low values of Ri are the result of a large baroclinicity or a small stratification

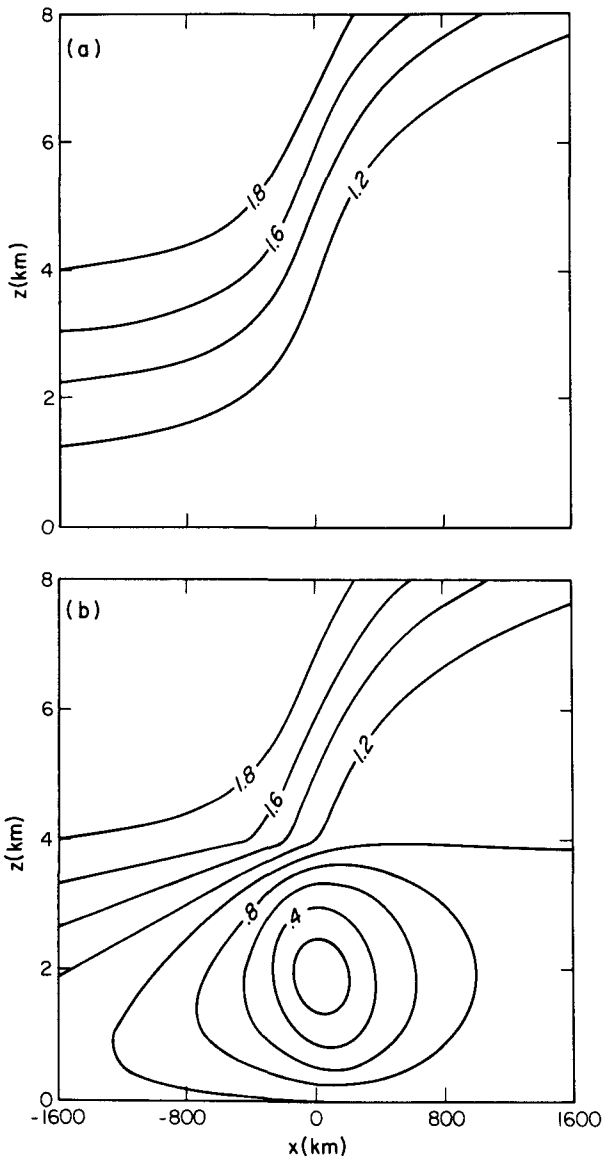

FIG. 9. Potential vorticity fields associated (a) with the front shown in Fig. 8a and (b) with the front shown in Fig. 8d.

or both. It follows that the Ri field is an important diagnostic field that contains much information regarding the intensity, structure, and the stability spectrum of the front (Moore and Peltier 1987, 1989a,b). In Fig. 10, presented are the Richardson number fields associated with the frontal zones of Fig. 8a, d. As previously described, the frontal zone in the no heating case is reasonably symmetric about the axis of maximum baroclinicity. This symmetry is reflected in its Ri field, Fig. 10a. The dramatic symmetry breaking that results from surface heating can be clearly seen in the Ri field shown in Fig. 10b. Surface heating has resulted in a pronounced reduction in the minimum Ri, an extension of the region of low Ri into the cold air, a tightening of the gradient of Ri on the warm side of the front. The overall structure of the Ri field shows the same "hook shape" that is present in the observations on Reed and Duncan (1987) as illustrated in Fig. 1b.

4. Discussion and conclusions

In this paper, the geostrophic momentum approximation has been employed to the primitive equations in order to investigate the effects that surface heating has on deformation induced frontogenesis. The primary difficulty in solving this problem is that the two diagnostic fields, potential vorticity and temperature,

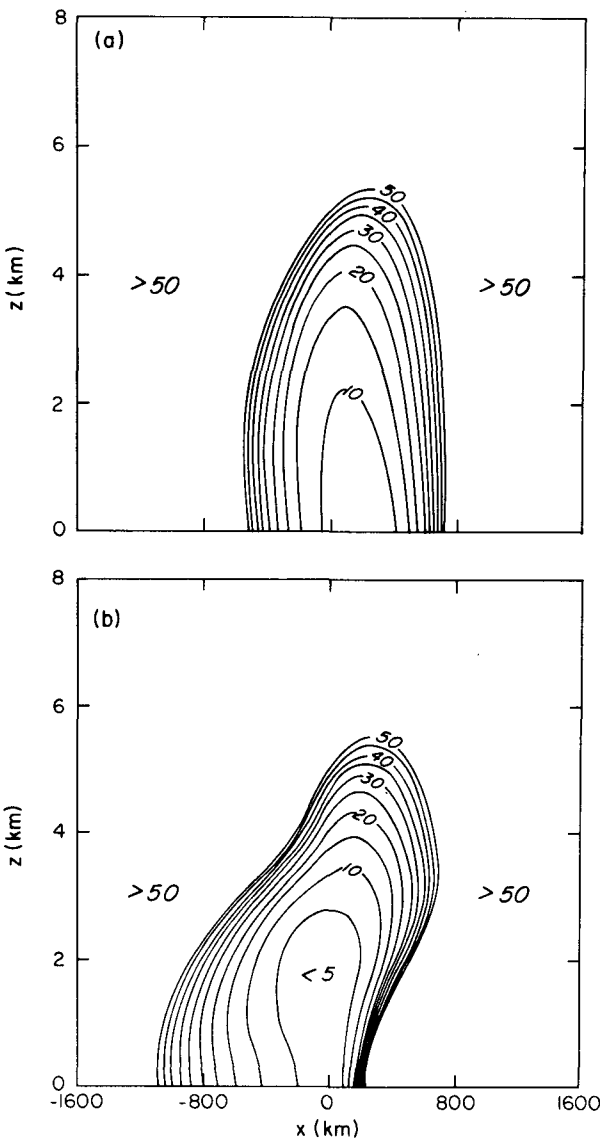

FIG. 10. As in Fig. 9, but for the Richardson number fields.

are not conserved following the fluid motion. By adopting a Lagrangian perspective, it has been possible to nevertheless develop a particularly simple approach that allows for the solution of this problem.

The model developed is capable of describing either adiabatic or diabatic frontogenesis which occurs in either a constant or nonuniform potential vorticity fluid. It was tested by considering the special case of adiabatic frontogenesis in a constant potential vorticity fluid. For this case, time enters into the problem only in terms of an integrated amount of deformation. Experiments using different deformation rates indicated that the Lagrangian model did indeed satisfy this important constraint. Furthermore, a comparison of the analytic solution, which exists for this case, with that obtained with the Lagrangian model showed that there were no significant differences between the two.

Having established the validity of the Lagrangian model, the next step was to investigate the effects that surface heating has on frontogenesis. As described in the Introduction, fronts that have been subject to strong surface heating have a profoundly different structure to those that are produced by means of adiabatic frontogenesis. The most important structural modifications include: the development of a highly asymmetric low-level jet; the presence of an isothermal region in the vicinity of the jet maximum; an enhancement of the horizontal temperature gradient on the cold side of the jet; and an extension of the region of low Ri into the cold air.

As it has been demonstrated in this paper, the inclusion of a parameterization of surface sensible heat flux allows one to generate frontal zones that have all the structural characteristics previously described. Furthermore, it has been shown that the modifications that arise are particularly sensitive to the choice for the surface temperature distribution. Use of a constant surface temperature resulted in a reduction in the maximum baroclinicity associated with the front. In contrast, the use of a spatially varying surface temperature distribution led to a marked increase in the maximum baroclinicity. In all cases, surface heating was responsible for a reduction in the minimum static stability. It was also found that there was no significant difference between the fronts that were subject to surface heating after deformation induced frontogenesis had ceased and those that subject to it during active frontogenesis.

This investigation was motivated by the observations discussed by Reed and Duncan (1987) of a frontal zone that had been modified by surface heating. As described in the Introduction, that particular front formed in a region that was characterized by strong gradient in the surface temperature. It, thus, corresponds to the model runs in which there was a nonuniform surface temperature distribution of the form previously described. Indeed, the best overall comparison of the fronts that formed in this model with the observations occurred for those runs in which this was the case. In particular, the front illustrated in Fig. 8d has a structure that is remarkably similar to that observed by Reed and Duncan (1987) shown in Fig. 1. Both fronts share the same characteristics described above. In addition, both the along-front velocity fields have a pronounced tilt to the east (positive x) with height. This tilt also is present in their Richardson number fields (Figs. 1b and 11b). Furthermore, both fronts have a distinctive hook shape to their Richardson number fields.

As shown, surface heating can lead to both an increase in the maximum baroclinicity and a reduction in the minimum stratification associated with a frontal zone. As described by Moore and Peltier (1987, 1989a), both of these effects are expected to result in an increase in the rate at which frontal instabilities can grow. Moore and Peltier (1989b) have demonstrated that the family of polar lows that developed along the Reed and Duncan frontal zone were the result of one such frontal instability. One can assert that the rapid growth of these disturbances (doubling times on the order of 12 hours) is the result of the effects, i.e., an increase in baroclinicity and a reduction in static stability, that surface heating had on the frontal zone along which they developed. This then provides for an *indirect mechanism* by which surface heating contributes to the development of cyclonic disturbances by modifying the background flow rather than by direct interaction with the growing cyclone.

Acknowledgments. The research described in this paper was funded by a grant from CRAY Research, Inc. The computations were performed at the Ontario Centre for Large Scale Computation. The author would like to thank K. P. Bowman for his assistance in developing the multigrid solver used in this paper.

REFERENCES

Akima, H., 1978: A method of bivariate interpolation and smooth surface fitting for irregularly distributed data points. *ACM Trans. Math. Software,* **4,** 148–159.

Blumen, W., 1980: A comparison between the Hoskins–Bretherton model of frontogenesis and the analysis of an intense surface frontal zone. *J. Atmos. Sci.,* **37,** 64–77.

Brandt, A., 1985: *Guide to Multigrid Development in 'Multigrid Methods.'* Springer-Verlag, 120 pp.

Buzzi, A., A. Trevison and G. Salustri, 1981: Internal frontogenesis: a two-dimensional model in isentropic, semigeostrophic coordinates. *Mon. Wea. Rev.,* **109,** 1053–1060.

Chan, D. S. T., 1988: Mesoscale anomalies and rainband formation. Ph.D. thesis, University of Toronto, 133 pp.

Cullen, M. J. P., 1983: Solutions to a model of a front forced by deformation *Quart. J. Roy. Meteor. Soc.,* **109,** 565–573.

——, 1989: On the incorporation of atmospheric layer effects into a balanced model. *Quart. J. Roy. Meteor. Soc.,* **115,** 1109–1131.

——, and R. J. Purser, 1984: An extended Lagrangian theory of semigeostrophic frontogenesis. *J. Atmos. Sci.,* **41,** 1477–1497.

Forbes, G. S., and W. D. Lottes, 1985: Classification of mesoscale vortices in polar airstreams and influence of large-scale environment on their evolution. *Tellus,* **37A,** 132–155.

Fritts, M. J., and J. P. Boris, 1979: The Lagrangian solution of transient problems in hydrodynamics using a triangular mesh. *J. Comput. Phys.,* **31,** 173–215.

Gill, A. E., 1982: *Atmosphere–Ocean Dynamics,* Academic Press.

Hoskins, B. J., 1971: Atmospheric frontogenesis models: Some solutions. *Quart. J. Roy. Meteor. Soc.,* **97,** 139–153.

——, and F. P. Bretherton, 1972: Atmospheric frontogenesis: mathematical formulation and solution. *J. Atmos. Sci.,* **29,** 11–37.

——, and N. V. West, 1979: Baroclinic waves and frontogenesis. Part II: Uniform potential vorticity jet flows—cold and warm fronts. *J. Atmos. Sci.,* **36,** 1663–1680.

Mak, M., and P. R. Bannon, 1984: Frontogenesis in a moist semigeostrophic model. *J. Atmos. Sci.,* **41,** 3485–3500.

Mansfield, D. A., 1974: Polar lows. The development of baroclinic disturbances in cold air outbreaks. *Quart. J. Roy. Meteor. Soc.,* **100,** 541–554.

Moore, G. W. K., 1987: Frontogenesis in a continuously varying potential vorticity fluid. *J. Atmos. Sci.,* **44,** 761–770.

——, and W. R. Peltier, 1987: Cyclogenesis in frontal zones. *J. Atmos. Sci.,* **44,** 384–409.

——, and ——, 1989a: Nonseparable baroclinic instability. Part I: Quasi-geostrophic dynamics. *J. Atmos. Sci.,* **46,** 57–78.

——, and ——, 1989b: On the development of polar low wavetrains in "Polar and Arctic Lows." P. F. Twitchell, E. A. Rasmussen and K. L. Davidson, Eds., Depack, 141–153.

Peltier, W. R., G. W. K. Moore and S. M. Polavarapu, 1990: Frontogenesis and cyclogenesis. *Tellus,* **42A,** 3-13.

Rasmussen, E., 1985: A case study of polar low development over the Barents Sea. *Tellus,* **37A,** 407–418.

Reed, R. J., and C. N. Duncan, 1987: Baroclinic instability as a mechanism for the serial development of polar lows: a case study. *Tellus,* **39A,** 376–384.

Thorpe, A. J., and K. A. Emanuel, 1985: Frontogenesis in the presence of small stability to slantwise convection. *J. Atmos. Sci.,* **42,** 1809–1824.

Williams, R. T., L. C. Chou and C. J. Cornelius, 1981: Effects of condensation and surface motion on the structure of steady-state fronts. *J. Atmos. Sci.,* **38,** 2365–2376.

Wu, R., and W. Blumen, 1982: An analysis of Ekman boundary layer dynamics incorporating the geostrophic momentum approximation. *J. Atmos. Sci.,* **39,** 1774–1782.

Young, J. A., 1973: A theory for isallobaric air flow in the planetary boundary layer. *J. Atmos. Sci.,* **30,** 1584–1592.